Corrosion Science 52 (2010) 3917–3923

Contents lists available at ScienceDirect

Corrosion Science

journal homepage: www.elsevier.com/locate/corsci

The influence of carbon nanotubes on the corrosion behaviour of AZ31B magnesium alloy

Hiroyuki Fukuda [a,b,*], Jerzy A. Szpunar [c], Katsuyoshi Kondoh [d], Richard Chromik [a]

[a] Department of Mining Metals and Materials Engineering, McGill University, The Wong Building, 3610 University Ave., Montreal, Canada H3A 2B2
[b] Graduate School of Engineering, Osaka University, 1 Yamadaoka, Suita, Osaka 565-0871, Japan
[c] Department of Mechanical Engineering, University of Saskatchewan, 57 Campus Drive, Saskatoon, SK, Canada S7N 5A9
[d] Joining and Welding Research Institution, Osaka University, 11-1 Mihogaoka, Ibaraki, Osaka 567-0047, Japan

ARTICLE INFO

Article history:
Received 25 June 2010
Accepted 7 August 2010
Available online 11 August 2010

Keywords:
A. Magnesium
A. Metal matrix composites
B. Polarization
B. Weight loss
C. Anodic dissolution
C. Interfaces

ABSTRACT

Carbon nanotubes (CNTs) are an effective reinforcement for magnesium (Mg) and its alloys due to their excellent mechanical properties. However, due to their quite different electrical properties compared to other carbon allotropes, the influence of CNTs on the corrosion of Mg is expected to be different. For this reason, the corrosion of AZ31B Mg alloy based composite with CNTs (AZ31B/CNT composite) was investigated with immersion tests, polarization tests and surface potential measurements. The galvanic corrosion between the Mg matrix and CNTs played an important role in the corrosion behaviour of the AZ31B/CNT composite.

© 2010 Elsevier Ltd. All rights reserved.

1. Introduction

Magnesium (Mg) alloys, due to their low density of 1.738 g/cm^3 find applications in various structural and mechanical components. It is widely recognized that replacing the conventional structural materials such as steels or aluminium alloys with Mg alloys can significantly reduce the fuel consumption of the transportation vehicles [1]. However, some difficulties such as poor corrosion resistance, low mechanical properties, and low formability have been limited the application of Mg and its alloys. In terms of the corrosion resistance, quite low standard electrode potential (SEP) of −2.36 V [2] highly accelerates the corrosion of Mg and its alloys. When Mg contacts with other nobler elements, ignoble Mg must be anode in the galvanic cell formed between Mg and nobler elements [3]. For example, iron (Fe), nickel (Ni), and copper (Cu), only with a few hundreds ppm, rapidly enhance the corrosion rate of Mg matrix [4]. Since these elements are usually introduced as contaminations, with careful avoidance of these elements in fabricating steps, at present, more or less anti-corrosive high purity Mg and its alloys are produced.

On the other hand, for wider use of Mg and its alloys, mechanical properties of the conventional Mg alloys must be improved. At the moment, the ultimate tensile strength of the mould casting AZ91C Mg alloy is only 275 MPa [5] while that of the casting AZ6N4 aluminium (Al) alloy is 540 MPa [6]. One strategy to improve the mechanical properties of Mg alloys is the fabrication of Mg alloy based metal matrix composites (Mg-MMCs). Though lots of kinds of reinforcements have been tested so far, carbon nanotubes (CNTs) which is one of carbon allotropes having cylindrical shape of scrolled graphen sheets [7], and with sizes ranging from 10–100 nm diameter and up to a few micrometer length, have been considered as one of the superior reinforcement materials in Mg-MMC because of their exceptional mechanical properties. For instance, their Young's modulus is around 4 TPa [8] compared to only 44 GPa for pure Mg [5]. Thus, many attempts have been made to produce Mg-MMC with CNTs to improve mechanical properties of various Mg alloys [9–14]. In spite of the difficulty in the segregation of CNT bundles caused by its own van der Waals force, some recent studies succeeded to improve mechanical properties of Mg alloys with CNTs [9,10,14].

Meanwhile, elemental carbon, which is a much nobler element than elemental Mg [2], harms the corrosion resistance of Mg. Hall reported that PAN-based carbon fibre deteriorated Mg corrosion resistance due to the formation of galvanic cell between the Mg matrix and carbon fibre [15]. However, CNTs show quite different electrical properties from other carbon allotropes [16]. Thus, the effect of CNTs on Mg corrosion phenomenon is expected to be different from that of other carbon allotropes. In the previous study, Endo et al. reported that the corrosion resistance of AZ91D Mg-MMC with CNTs (AZ91D/CNT composite) was improved compared to

* Corresponding author. Address: Graduate School of Engineering, Osaka University, 1 Yamadaoka, Suita, Osaka 565-0871, Japan. Fax.: +81 06 68798669.
E-mail address: fukkun-fukuda@jwri.osaka-u.ac.jp (H. Fukuda).

0010-938X/$ - see front matter © 2010 Elsevier Ltd. All rights reserved.
doi:10.1016/j.corsci.2010.08.009

that of pristine AZ91D [17]. In their report, it was claimed that CNTs act as a water repellent and reinforce the surface protective layers. Though both phenomena should enhance the corrosion resistance, no specific effort was made to explore the role of galvanic corrosion between Mg matrix and CNTs. On the other hand, Aung et al. reported that the corrosion resistance of pure Mg composite with CNTs was decreased compared to that of pristine pure Mg by measuring hydrogen evolution and mass loss during immersion tests, and polarization curves in 3.5 wt.% NaCl solution [18]. They concluded that the corrosion resistance of pure Mg composite with CNTs was deteriorated due to the galvanic corrosion between the Mg matrix and CNTs. However, they did not investigate the role of CNTs on the local corrosion behaviour of the Mg matrix, neither. The influence of CNTs on the corrosion behaviour of Mg matrix remains unclear. Hence, in this study, first overall corrosion behaviour of AZ31B Mg alloy based composite with CNT (AZ31B/CNT composite) was evaluated with immersion tests, and then, the role of CNTs on the corrosion behaviour of the Mg matrix was investigated with polarization tests and surface potential measurements.

2. Experimental

2.1. Fabrication of AZ31B/CNT composites

AZ31B Mg alloy powders with 97 μm mean diameter and multi-walled CNTs with 13–16 nm outer diameter and 1–10 μm length, as shown in Fig. 1, were prepared as raw materials. The chemical compositions of the AZ31B Mg alloy powders are Al, 2.95; Zn, 1.03; Mn, 0.21; Si, 0.012; Fe, 0.0048 mass%. With these materials, AZ31B/CNT composite was fabricated through two steps: the CNT-coating step with the solution containing zwitterionic surfactant, which is the surface active agent having both negative and positive charges at the tip of its hydrophilic groups, and the consolidation step with spark plasma sintering (SPS) technique [19]. In the CNT-coating steps, CNT coating on the powder surface was conducted as the schematic illustration shown in Fig. 2. First, AZ31B raw powders were dipped into and taken out from the aqueous solution containing the zwitterionic surfactant, 3-(*N*,*N*-dimethyl stearyl ammonio) propane sulfonate, with 1 and 3 mass% CNTs. The details about how CNT bundles were disassembled in the solution are given in another reference [20]. Then, these powders were kept in argon (Ar) gas atmosphere at 80 °C for 2 h to dry the surface. At this point, these powders were coated with not only

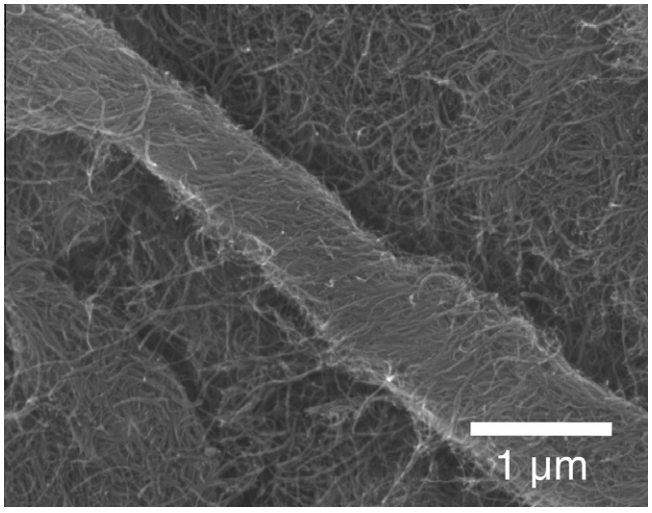

Fig. 1. The scanning electron microscopy (SEM) observation on the as-received CNTs.

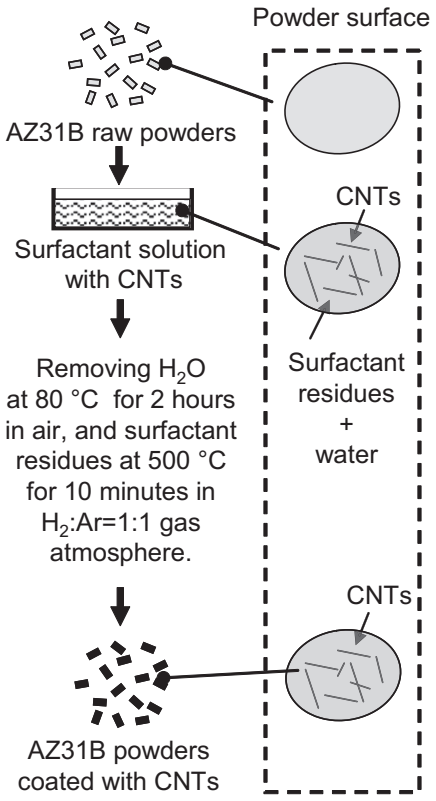

Fig. 2. The schematic illustration of the preparation steps of the AZ31B powders coated with CNTs. As-received powders were dipped into and taken out from the surfactant solution with CNTs, dried at 80 °C for 2 h in air, and then, heat treated at 500 °C for 10 min in H2:Ar = 1:1 gas atmosphere.

CNTs but also surfactant residues which obstruct powders from bonding together in the consolidation steps. Therefore, heat treatment was employed at 500 °C for 10 min in hydrogen (H_2):Ar = 1:1 gas atmosphere to thermally remove the surfactant residues. After the heat treatment, the content of carbon in the CNT-coated powders were measured with Inert gas fusion instruments-carbon–sulphur determination (LECO Co., CS-200) technique. This carbon content was regarded as the content of CNTs in each sample as the previous study [21]. Subsequently, the CNT-coated powders were consolidated in carbon die (diameter; 43 mm) at 550 °C for 30 min under 30 MPa pressure in vacuum with SPS equipment (Syntech Co., SPS-1030S). Due to the nature of the fabrication process, CNTs were distributed only at the primary particle boundaries in the specimens. Thus, at a very local level, the distribution of CNTs might be considered heterogeneous. However, since the mean particle diameter of Mg, 97 μm, is much less than the entire specimen area exposed to the corrosion media, we expect that the distribution of CNTs is homogenous at the scale studied for the overall corrosion analysis. For convenience, fabricated samples were coded depending on their content of CNTs as indicated in Table 1. Their bulk densities, which were calculated from their weight and volume, were also listed in Table 1. As the corrosion resistance of the composites should be discussed around the con-

Table 1
The sample code, the CNT content and the bulk density of each sample.

Code	CNT content (vol.%)	Bulk density (%)
a*	0	98.24
b	0.89	97.69
c	2.66	96.92

* AZ31B pristine material.

tent of CNTs at which the mechanical properties are expected to be improved, the content of CNTs in this study, 0.89 vol.% and 2.66 vol.%, was determined corresponding to that of the previous research which reported that yield stress of pure Mg/CNT composite and AZ31B/CNT composite were, with approximately 1 vol.% of CNTs, improved about 34–42% and 24–27%, respectively [9].

2.2. Evaluation of the corrosion behaviour of AZ31B/CNT composite

Immersion tests were performed to investigate the overall corrosion resistance of each sample. All samples were cut into cylindrical specimens having 10 mm height and 12 mm diameter. Specimens were immersed into 1200 ml of 0.51 M sodium chloride (NaCl) solution at pH = 6.2. The solution was deaerated and agitated with 1000 ml/min Ar gas flow. Throughout the immersion tests, the pH changes of the test solutions were collected in the intervals of 1 h with pH meter. To increase the credibility of the tests, the tests were repeated twice under the same condition. The Mg reaction with deaerated aqueous solution is expressed in the equation below [22].

$$Mg(s) \rightarrow Mg^{2+}(aq) + 2e^- \text{ (anodic reaction)}$$
$$2H_2O + 2e^- \rightarrow H_2(g) + 2OH^-(aq) \text{ (cathodic reaction)}$$
$$Mg^{2+}(aq) + 2OH^-(aq) \rightarrow Mg(OH)_2(s) \text{ (corrosion product)}$$

When the Mg matrix dissolves, hydroxide ions (OH^-) are released into the test solution. The more Mg dissolves into the solution, the higher solution pH value can be expected. Mass loss was also calculated by weighing specimens before and after the test. When Mg matrix dissolves into the test solution, specimens should lose its mass corresponding to the mass of dissolved Mg. Therefore, the specimen experienced severer corrosion loses greater mass after the immersion test.

The polarization test was carried out to investigate whether the galvanic corrosion progressed in AZ31B/CNT composite. The samples were cut into square specimens (15 mm × 15 mm × 3 mm), and ground in ethanol with #600 and #1200 silicon carbide (SiC) abrasive papers. After the grinding processes, the specimens were cleaned in ethanol using ultrasonic vibration. Since Mg easily reacts with water and creates magnesium hydroxide ($Mg(OH)_2$), the contact of specimens with water was avoided at all specimen preparation steps. The specimens were immersed into 75 ml of 0.017 M NaCl solution at pH = 6.47 for 1 h to stabilize the sample surface. Since, with the solution for the immersion tests containing 0.51 M Cl^- ions, all specimen surface was too corroded to understand where CNTs existed, the less corrosive solution containing 0.017 M Cl^- ions was used in this test. The solution pH value was adjusted at 12 by using sodium hydroxide (NaOH) to emphasize the galvanic corrosion progressed in samples by reducing the uniform dissolution of Mg matrix. While Cl^- ions breaks down the surface protective film, the film could be more or less effective in the alkaline solution used in this study since the concentration of Cl^- in the test solution was low, 0.017 M. Although, as an alloying element, the AZ31B contains Al, whose passivation film of $Al(OH)_3$ was unstable at alkaline pH value [23,24], all Al was solutionized into Mg matrix in AZ31B used in this test. Thus, the specimen surface exposed to the test solution did not contain Al phase, so entire specimen surface was protected with stable passivation film during the tests. The polarization curves were measured at the scanning ratio of 1 mV/s with a laboratory potentiostat (AUTOLABO model PGSTAT 302). A saturated calomel electrode (SCE) as a reference electrode and a graphite rod as a counter electrode, were submerged into the test solution. The specimen was exposed to the test solution by fixing it to a window of the plastic container; no other material was in the test solution except a specimen, SCE, and a graphite rod throughout the tests. The cathode/anode area ratio (7.66) and the distance between cathode and anode (45 mm) were kept constant during this test. The polarization test was repeated twice to validate the test results. The surface potential difference (SPD) between Mg and CNTs was calculated by measuring the surface potential between specimen and the needle at the tip of the cantilever attached to the Scanning Kelvin Probe Force Microscope (SKPFM) [25]. The needle was coated with platinum iridium5 ($PtIr_5$) to conduct electrons. The surface potential was defined by the expression below.

$$\text{Surface potential} = (\Phi_{PtIr5} - \Phi_{specimen})/e$$

where e is an electrical charge, and Φ_{PtIr5} and $\Phi_{specimen}$ are the work function of $PtIr_5$ and specimen, respectively. In the previous research, Schmutz and Frankel reported the proportional relationship between surface potential and SEP in NaCl aqueous solution [26]. Therefore, the surface potential measurement provides the basic knowledge whether the driving force is enough to provoke the local corrosion. Meanwhile, SKPFM measures the surface potential between the cantilever needle and specimen as described above. That is, the measured surface potential becomes low when the SEP of the measured surface is high. The SPD between two phases on the specimen surface is defined as an expression below.

$$SPD = V_{SHE,2} - V_{SHE,1} = (\Phi_{PtIr5} - \Phi_2)/e - (\Phi_{PtIr5} - \Phi_1)/e = (\Phi_1 - \Phi_2)/e$$

$SPD = V_{SHE,2} - V_{SHE,1} = (\Phi_{PtIr5} - \Phi_2)/e - (\Phi_{PtIr5} - \Phi_1)/e = (\Phi_1 - \Phi_2)/e$, where $V_{SHE,1}$, $V_{SHE,2}$, Φ_1 and Φ_2 is the surface potential of phase 1, that of phase 2, the work function of phase 1 and that of phase 2, respectively. For the SKPFM scanning, the specimen (10 × 10 mm square) was ground with #2000 and #4000 SiC abrasive papers, and polished with 0.25 μm diamond pastes. The specimen surface was rinsed in ethanol using ultrasonic vibration after the polishing. After the SPD measurement, specimens were corroded in 0.017 M NaCl solution at pH = 6.02 for 5 min to investigate the surface morphology around CNTs after corrosion. Throughout this study, the surface conditions were characterized with field emission scanning electron microscopy (FE-SEM, JOEL, JSM-6500F) equipped with energy dispersive X-ray spectroscopy (EDS, JEOL, JED-2300) system. X-ray diffraction (XRD) system with copper (Cu) tube was also operated to identify the structure of compounds formed after the immersion tests.

3. Results and discussion

3.1. Overall corrosion behaviour of AZ31B/CNT composite

Fig. 3 shows the appearance of sample a and c at 1, 6 and 12 h from the beginning of the immersion. Sample c was severely corroded after 6 h-immersion while sample a kept its original shape even after 12 h-immersion. Sediments around sample c after 12 h-immersion were scanned with XRD as indicated in Fig. 4. The XRD profile identified the sediments as the mixture of $Mg(OH)_2$ and few amount of aluminium hydroxide ($Al(OH)_3$). As widely recognized, Mg produces $Mg(OH)_2$ when it reacts with water or moisture. Thus, the sediments were considered as the detached corrosion products detached from specimen surface due to the harsh H_2 gas evolution of the cathodic reaction. Though, in the XRD profile, $Al(OH)_3$ was identified as well, it was usually included in the surface corrosion products of AZ31 as Wang et al. reported in the previous report [27].

The pH changes during the immersion test were shown in Fig. 5. The pH values of sample b and c increased faster and reached higher values than that of sample a. This means that the Mg matrix of sample b and c was corroded faster and greater into the test solution. The pH value of sample c with CNTs stabilized around pH = 11 after approximately 3 h from the beginning of the immersion. This

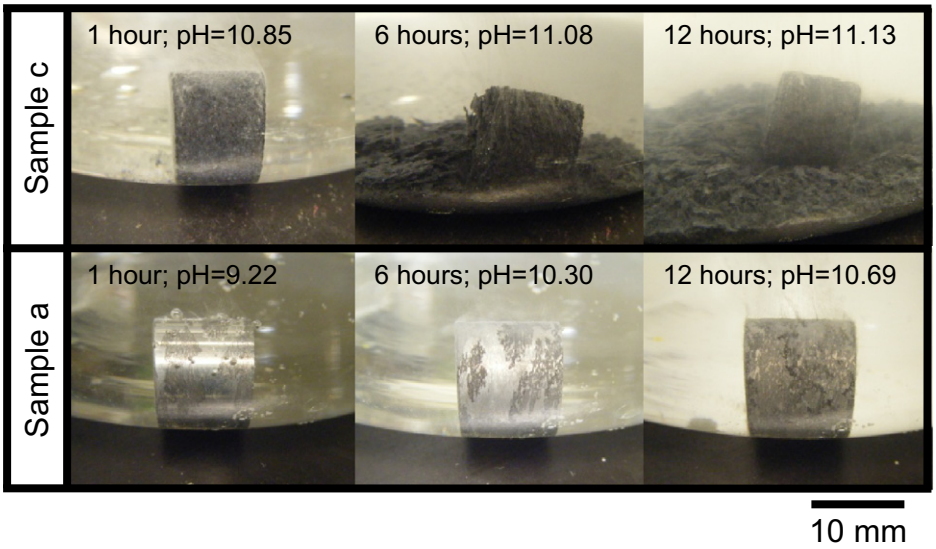

Fig. 3. The photos of sample c and a during the immersion test in 0.51 M NaCl solution with Ar gas flow. The sample c was severely corroded after 6 h although the sample a did not show such serious corrosion even after 12 h.

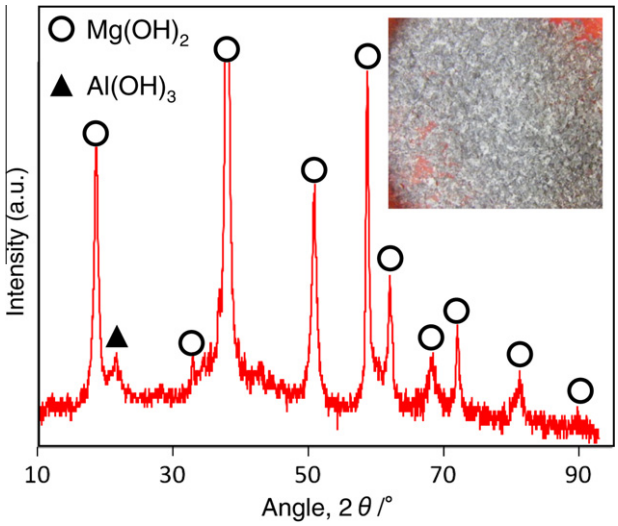

Fig. 4. The XRD profile of the sediments accumulated around sample c after 12 h-immersion in 0.51 M NaCl solution. The sediments mainly consisted of Mg(OH)2, the main corrosion product of Mg in aqueous solution.

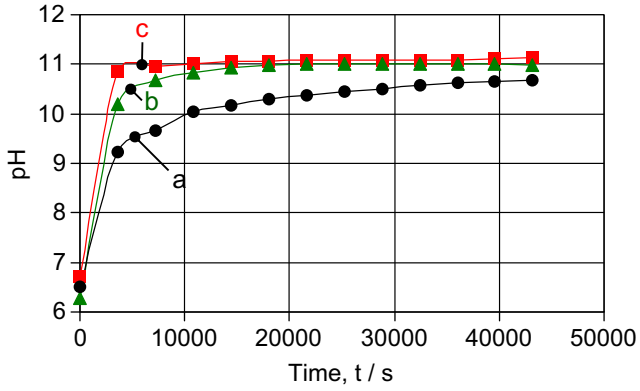

Fig. 5. The pH changes of each sample in 0.51 M NaCl solution with the Ar gas flow. In the figure, a, b, and c mean the sample without, with 0.89 and 2.66 vol.% CNTs, respectively. The pH values of sample b and c increased faster and to higher values at any time than that of samples a, the sintered pristine Mg alloy.

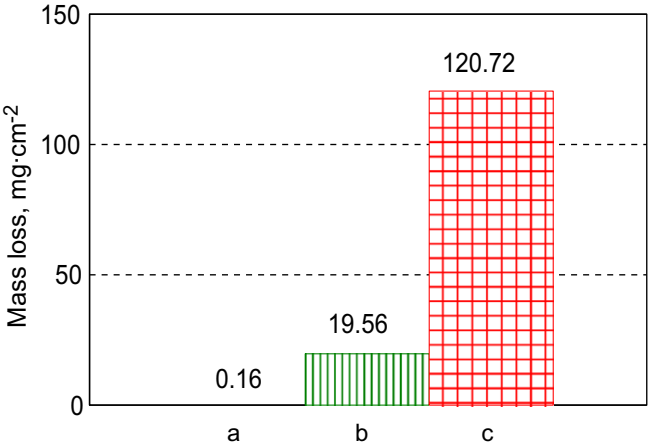

Fig. 6. The mass loss of each sample after 2 h-immersion in 0.51 M NaCl solution. In the figure, a, b, and c mean the sample without, with 0.89 and 2.66 vol.% CNTs, respectively. The mass loss of sample b and c was much greater than that of sample a, the sintered pristine Mg alloy.

phenomenon was also observed in sample b after approximately 6 h-immersion. These results suggests that, the test solution of sample b and c was almost saturated with $Mg(OH)_2$ at the beginning of the tests. Additionally, the sediments appeared around the corroded specimen after 6 h-immersion previously shown in Fig. 3. These sediments, which were mainly composed with $Mg(OH)_2$, also justified the $Mg(OH)_2$ saturation of the test solution at the beginning of the tests. On the other hand, the test solution pH value of sample a increased and few sediments were observed around the sample a as shown in Fig. 3 even after 12 h-immersion, so the test solution of sample a was not or just saturated with $Mg(OH)_2$ after 12 h-immersion. Hence, though the pH value of sample a approached to that of sample b and c at the end of the test, this is because the test solution of sample b and c was saturated with $Mg(OH)_2$ at the beginning of the tests. The earlier saturation of the test solution of sample b and c also indicated the fast Mg matrix dissolution. Moreover, the significant mass loss was calculated in sample b and c as shown in Fig. 6. Sample b and c lost their mass of 19.56 and 120.72 mg/cm^2 after immersion

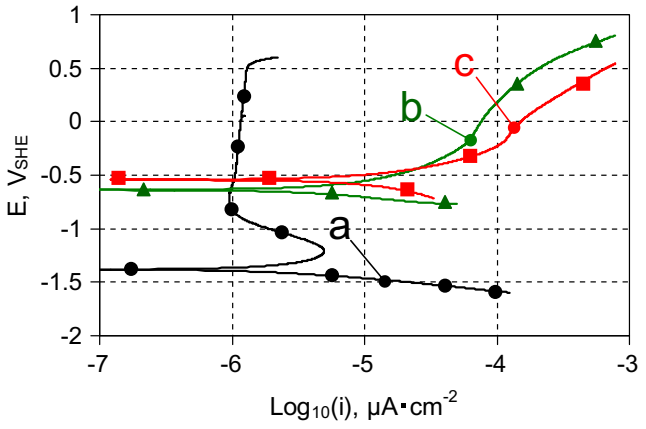

Fig. 7. The polarization curves of each sample at pH = 12 in 0.017 M NaCl solution. In the figure, a, b, and c means the sample without, with 0.89 and 2.66 vol.% CNTs, respectively. In sample b and c, the electropositive shift was approximately 0.7 V.

test, respectively despite that sample a lost only 0.16 mg/cm^2. Faster and greater Mg matrix dissolution of sample b and c caused greater mass loss. Surely, corrosion products, which increase the sample mass after the immersion test, might be stuck on the sample surface. However, the corrosion of these samples was quite sever, and the detachment of corrosion products was often observed everywhere on the specimen surface. Additionally, the corrosion product layer was not much thick compared to the amount of the deposited corrosion product. The metallic surface soon appeared when the corroded specimens were ground with SiC paper. Thus, the mass gain due to the surface corrosion products after the immersion test was insignificant compared to the mass loss caused by the mass of Mg matrix dissolved into the solution.

3.2. Investigations of the role of CNTs on the corrosion behaviour of Mg matirix

The polarization curves at pH = 12 are shown in Fig. 7. The corrosion potential of sample b and c positively shifted about 0.7 V from that of sample a. This electropositive shift indicates that the galvanic corrosion progressed in sample b and c. Besides, polarization curves of sample b and c did not exhibit any passivation behaviour. When the Mg reacts with the aqueous solution, usually, the corrosion products were left on the surface, and more or less, behaves as a protective film. However, sample b and c did not show such behaviour. The corrosion products on the surface were not effective in protecting Mg matrix from dissolution. The surface morphology of sample c after the polarization test was shown in Fig. 8 (a). The specimen surface was locally damaged at primary particle boundary, where lots of CNTs were present as shown in Fig. 8 (b). In the vicinity of CNTs, harsh corrosion progressed, and the surface protective film lost its effectiveness. The 2D and 3D surface potential distribution of sample c at the primary particle boundary was presented in Fig. 9 (a) and (b), respectively. The primary particle boundary, the dark area, showed low surface potential; that means the high absolute potential. SPDs between Mg matrix and the dark area, A–B, C–D, and E–F, were calculated 1.06, 1.09, and 1.14 V, respectively although SPDs between tow points at matrix, G–H, was less than 0.01 V. On the other hand, SEM observation revealed the presence of CNTs at the primary particle boundary, as displayed in Fig. 9 (c). The high absolute potential at the primary particle boundary was due to the presence of CNTs. As a result, SPD between Mg matrix and CNTs were around 1.1 V. In the previous study, Takei et al. measured the SPD between AZ91D Mg matrix and Fe [28], which is the well-known harmful element for the corrosion resistance of Mg matrix due to the formation of the galvanic cell with Mg matrix [29]. They reported that the SPD between Mg matrix and Fe was 0.5 ~ 0.7 V. Furthermore, in some earlier studies, the SPD between Mg matrix and intermetallic compounds was measured [30–32]. For example, Andreatta et al. reported that the average SPD of AZ80 Mg matrix with Al_8Mn_5, Mg_2Si, and $Mg_{17}Al_{12}$ (β phase) were 257.3, 97, and 152.3 mV, respectively [30]. It is widely recognized that Al–Mn intermetallics and β phase behave like a cathode to the Mg matrix, and form the galvanic cell with the Mg matrix [32]. Compared to these prior studies, SPD between the Mg matrix and CNTs obtained in this study (1.1 V), was enough high to form the galvanic cell between them. Surface conditions before and after immersion into 0.017 M NaCl solution for 5 min were shown in Fig. 10 (a) and (b), respectively. Same areas were observed to easily compare the surface morphology before and after the immersion test. In Fig. 10 (b), white debris were concentrated along the primary particle boundaries, where CNTs were located. Since the morphology of white debris was quite similar to the corrosion product, $Mg(OH)_2$, observed after the immersion test in 0.51 M NaCl solution identified with XRD in Fig. 4, the white debris can be regarded as the corrosion products piled up around CNTs. Obviously, due to the strong galvanic corrosion at the interfaces between the Mg matrix and CNTs, large amount of corrosion products were accumulated in the vicinity of CNTs.

4. Conclusion

The formation of the galvanic cell between the Mg matrix and CNTs due to the high potential difference (1.1 V), decreased the corrosion resistance of the AZ31B Mg alloy. Throughout the immersion tests, the pH values of the test solution for AZ31B/CNT composite increased rapidly and reached higher value than

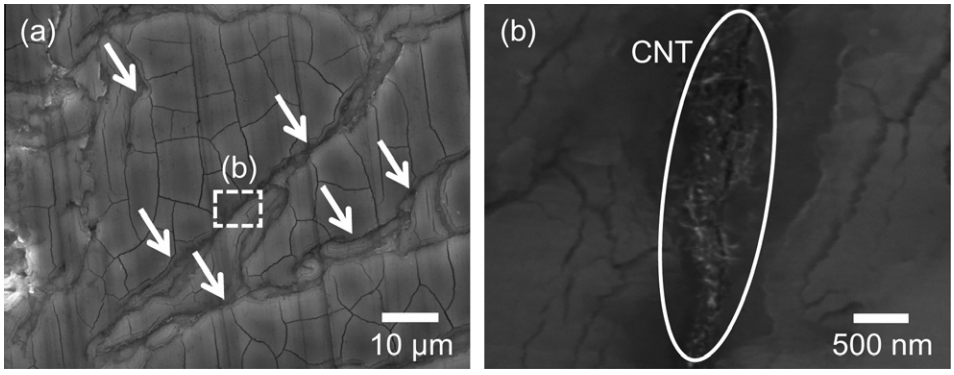

Fig. 8. The corroded surface of sample a after the polarization test at pH = 12 in 0.017 M NaCl solution. The severely corroded areas were locally observed along the primary particle boundary (a), where individual CNTs were present (b).

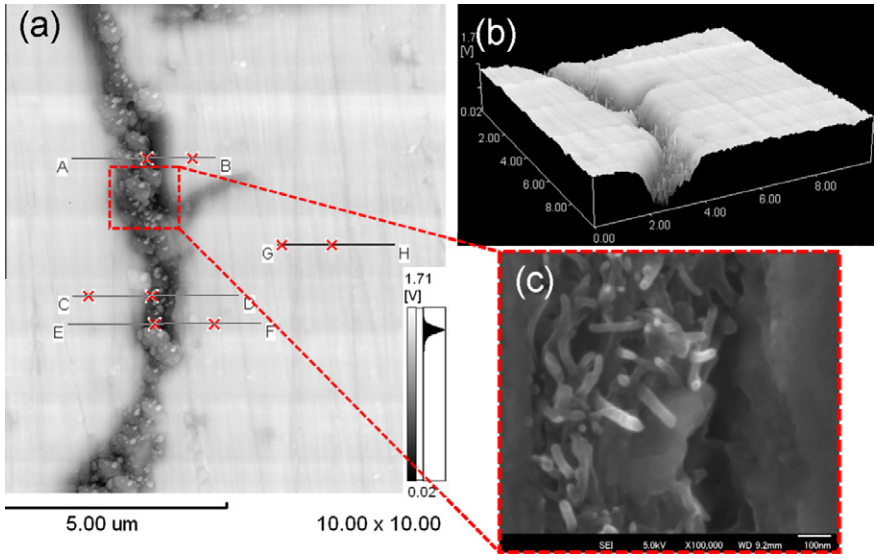

Fig. 9. The 2D and 3D surface potential distribution of sample c, (a) and (b), respectively, and CNTs at the primary particle boundary, (c). Large SPD was observed between Mg matrix and CNTs.

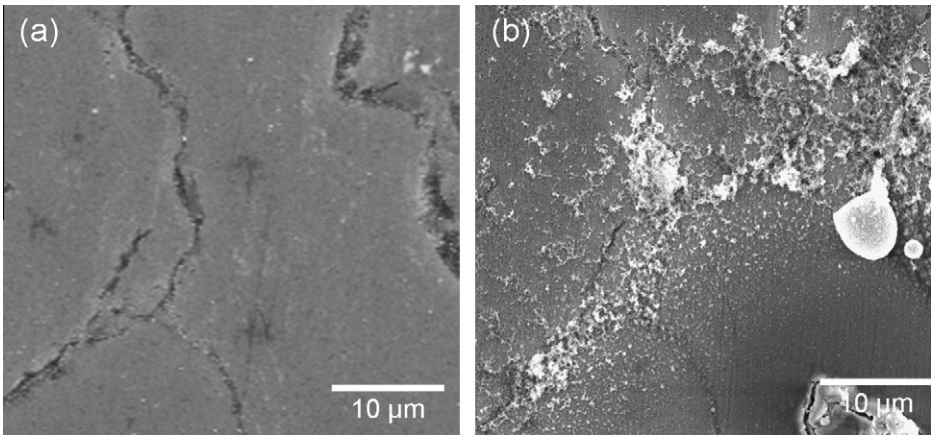

Fig. 10. Surface conditions of sample c before (a) and after (b) immersion test in 0.51 M NaCl solution for 5 min. The corrosion products were accumulated around CNTs after immersion test as a result of the formation of the strong galvanic cell between Mg matrix and CNTs.

that of the pristine sintered AZ31B Mg alloy. The significant mass loss of AZ31B/CNT composites was measured after immersion in 0.51 M NaCl as well. Corrosion potential of AZ31B/CNT composites sifted 0.7 V positively compared to that of AZ31B pristine material; that gave the information of progression of the galvanic corrosion inside of AZ31B/CNT composite. Surface potential measurement with SKPFM revealed 1.1 V SPD between Mg matrix and CNTs. The corrosion products were observed around CNTs after the immersion test in 0.017 M NaCl aqueous solution. Due to the strong driving force (1.1 V), the galvanic cell was constructed between Mg matrix and CNTs, and large amount of corrosion products were piled up in the vicinity of CNTs.

References

[1] J.T. Carter, P.E. Krajewski, R. Verma, The hot blow forming of AZ31 Mg sheet: formability assessment and application development, JOM Journal of the Minerals Metals and Materials Society 60 (2008) 77–81.
[2] D.A. Jones, Principles and prevention of corrosion, second ed., Prentice Hall, London, 1996.
[3] E. Ghali, W. Dietzel, K.U. Kainer, General and localized corrosion of magnesium alloys: a critical review, Journal of Materials Engineering and Performance 13 (2004) 7–23.
[4] J. Hillis, P. Kurze, Corrosion and surface protections, in: H.E. Friedrich, B.L. Mordike (Eds.), Magnesium technology: metallurgy, design data, applications, Springer, New York, 2006, pp. 473–497.
[5] B.L. Mordike, P. Lukác, Physical metallurgy, in: H.E. Friedrich, B.L. Mordike (Eds.), Magnesium technology: metallurgy, design data, applications, Springer, New York, 2006, pp. 63–107.
[6] V.S. Zolotorevsky, N.A. Belov, M.V. Glazoff, Casting aluminium alloys, Elsevier, Amsterdam, 2007.
[7] S. Iijima, Helical microtubules of graphitic carbon, Nature 354 (1991) 56–58.
[8] K. Mylvaganam, L.C. Zhang, Important issues in a molecular dynamics simulation for characterising the mechanical properties of carbon nanotubes, Carbon 42 (2004) 2025–2032.
[9] K. Kondoh, H. Fukuda, J. Umeda, H. Imai, B. Fugetsu, M. Endo, Microstructural and mechanical analysis of carbon nanotube reinforced magnesium alloy powder composites, Materials Science and Engineering A 527 (2010) 4103–4108.
[10] Y. Shimizu, S. Miki, T. Soga, I. Itoh, H. Todoroki, T. Hosono, K. Sakaki, T. Hayashi, Y.A. Kim, M. Endo, S. Morimoto, A. Koide, Multi-walled carbon nanotube-reinforced magnesium alloy composites, Scripta Materialia 58 (2008) 267–270.
[11] C.S. Goh, J. Wei, L.C. Lee, M. Gupta, Ductility improvement fatigue studies in Mg-CNT nanocomposites, Composite Science and Technology 68 (2008) 1432–1439.
[12] Q.Q. Li, A. Viereckl, C.A. Rottmair, R.F. Singer, Improved processing of carbon nanotube/magnesium alloy composites, Composite Science and Technology 69 (2009) 1193–1199.
[13] C.S. Goh, J. Wei, L.C. Lee, A. Gupta, Simultaneous enhancement in strength and ductility by reinforcing magnesium with carbon nanotubes, Materials Science and Engineering A 423 (2006) 153–156.

[14] C.S. Goh, J. Wei, L.C. Lee, M. Gupta, Development of novel carbon nanotube reinforced magnesium nanocomposites using the powder metallurgy technique, Nanotechnology 17 (2006) 7–12.
[15] W. Hall, Corrosion of carbon magnesium metal matrix composites, Scripta Metallurgica 21 (1987) 1717–1721.
[16] T. Shimizu, H. Abe, A. Ando, Y. Nakayama, H. Tokumoto, Electrical conductivity measurements of a multi-walled carbon nanotube, Surface and Interface Analysis 37 (2005) 204–207.
[17] M. Endo, T. Hayashi, I. Itoh, Y.A. Kim, D. Shimamoto, H. Muramatsu, Y. Shimizu, S. Morimoto, M. Terrones, S. Iinou, S. Koide, An anticorrosive magnesium/carbon nanotube composite, Applied Physics Letters 92 (2008).
[18] N.N. Aung, W. Zhou, C.S. Goh, S.M.L. Nai, J. Wei, Effect of carbon nanotubes on corrosion of Mg-CNT composites, Corrosion Science 52 (2010) 1551–1553.
[19] E.A. Olevsky, S. Kandukuri, L. Froyen, Consolidation enhancement in spark-plasma sintering: impact of high heating rates, Journal of Applied Physics 102 (2007).
[20] B. Fugetsu, W.H. Han, N. Endo, Y. Kamiya, T. Okuhara, Disassembling single-walled carbon nanotube bundles by dipole/dipole electrostatic interactions, Chemistry letters 34 (2005) 1218–1219.
[21] K. Kondoh, T. Threrujirapapong, H. Imai, J. Umeda, B. Fugetsu, Characteristics of powder metallurgy pure titanium matrix composite reinforced with multi-wall carbon nanotubes, Composite Science and Technology 69 (2009) 1077–1081.
[22] J. Van Muylder, M. Pourbaix, Magnesium, in: M. Pourbaix (Ed.), Atlas of Electrochemical Equilibria in Aqueous Solution, Pergamon Press, Oxford, 1966, p. 139.
[23] K. Ishii, R. Ozaki, K. Kaneko, H. Fukushima, M. Masuda, Continuous monitoring of aluminium corrosion process in deaerated water, Corrosion Science 49 (2007) 2581–2601.
[24] M. Anik, P. Avci, A. Tanverdi, I. Celikyurek, B. Baksan, R. Gurler, Effect of the eutectic phase mixture on the anodic behaviour of alloy AZ91, Materials and Design 27 (2006) 347–355.
[25] M. Nonnenmacher, M.P. Oboyle, H.K. Wickramasinghe, Kelvin probe force microscopy, Applied Physics Letters 58 (1991) 2921–2923.
[26] P. Schmutz, G.S. Frankel, Characterization of AA2024-T3 by scanning Kelvin probe force microscopy, Journal of the Electrochemical Society 145 (1998) 2285–2295.
[27] L. Wang, T. Shinohara, B. Zhang, H. Iwai, Characterization surface products on AZ31 magnesium alloy in dilute NaCl solution, Journal of Alloys and Compounds 485 (2009) 747–752.
[28] R. Takei, H. Fukuda, H. Imai, J. Umeda, K. Kondoh, Corrosion phenomenon evaluation of Mg Alloys using surface potential difference measured by SKPFM, Magnesium Technology, TMS (2010) 169–172.
[29] J.X. Jia, A. Atrens, G. Song, T.H. Muster, Simulation of galvanic corrosion of magnesium coupled to a steel fastener in NaCl solution, Materials and Corrosion-Werkstoffe Und Korrosion 56 (2005) 468–474.
[30] F. Andreatta, I. Apachitei, A.A. Kodentsov, J. Dzwonczyk, J. Duszczyk, Volta potential of second phase particles in extruded AZ80 magnesium alloy, Electrochimica Acta 51 (2006) 3551–3557.
[31] M. Jonsson, D. Thierry, N. LeBozec, The influence of microstructure on the corrosion of AZ91D studied by scanning Kelvin probe force microscopy and scanning Kelvin probe, Corrosion Science 48 (2006) 1193–1208.
[32] D.B. Blucher, J.E. Svensson, L.G. Johansson, M. Rohwerder, M. Stratmann, Scanning kelvin probe force microscopy – a useful tool for studying atmospheric corrosion of MgAl alloys in situ, Journal of the Electrochemical Society 151 (2004) B621–B626.